

## The roles of aerosol direct and indirect effects in past and future climate change

Hiram Levy II,<sup>1</sup> Larry W. Horowitz,<sup>1</sup> M. Daniel Schwarzkopf,<sup>1</sup> Yi Ming,<sup>1</sup> Jean-Christophe Golaz,<sup>1</sup> Vaishali Naik,<sup>2</sup> and V. Ramaswamy<sup>1</sup>

Received 30 July 2012; revised 15 January 2013; accepted 16 January 2013; published 20 May 2013.

[1] Using the Geophysical Fluid Dynamics Laboratory's (GFDL's) fully coupled chemistry-climate (ocean/atmosphere/land/sea ice) model (CM3) with an explicit physical representation of aerosol indirect effects (cloud-water droplet activation), we find that the dramatic emission reductions (35%–80%) in anthropogenic aerosols and their precursors projected by Representative Concentration Pathway (RCP) 4.5 result in  $\sim 1^\circ\text{C}$  of additional warming and  $\sim 0.1\text{ mm day}^{-1}$  of additional precipitation, both globally averaged, by the end of the 21st century. The impact of these reductions in aerosol emissions on simulated global mean surface temperature and precipitation becomes apparent by mid-21st century. Furthermore, we find that the aerosol emission reductions cause precipitation to increase in East and South Asia by  $\sim 1.0\text{ mm day}^{-1}$  through the second half of the 21st century. Both the temperature and the precipitation responses simulated by CM3 are significantly stronger than the responses previously simulated by our earlier climate model (CM2.1) that only considered direct radiative forcing by aerosols. We conclude that the indirect effects of sulfate aerosol greatly enhance the impacts of aerosols on surface temperature in CM3; both direct and indirect effects from sulfate aerosols dominate the strong precipitation response, possibly with a small contribution from carbonaceous aerosols. Just as we found with the previous GFDL model, CM3 produces surface warming patterns that are uncorrelated with the spatial distribution of 21st century changes in aerosol loading. However, the largest precipitation increases in CM3 are colocated with the region of greatest aerosol decrease, in and downwind of Asia.

**Citation:** Levy, H. II, L. W. Horowitz, M. D. Schwarzkopf, Y. Ming, J.-C. Golaz, V. Naik, and V. Ramaswamy (2013), The roles of aerosol direct and indirect effects in past and future climate change, *J. Geophys. Res. Atmos.*, 118, 4521–4532, doi:10.1002/jgrd.50192.

### 1. Introduction

[2] As a result of the industrial revolution and population growth, total anthropogenic emissions of sulfur dioxide ( $\text{SO}_2$ ), the source gas for sulfate aerosol, black carbon (BC), and organic carbon (OC) have grown dramatically [e.g., Lamarque *et al.*, 2010]. However, all of the latest future projections expect very significant decreases in emissions of all three compounds [Meinshausen *et al.*, 2011]. A fundamental question to be explored is the role that these changing levels of aerosols have played in the past climate and will play in the future.

[3] The biggest uncertainty regarding the role of aerosols in climate is the actual magnitude of the “aerosol effect,” as

discussed by Shine *et al.* [1990], Charlson *et al.* [1992], and Shine *et al.* [1995] and reviewed in considerable detail in both the Intergovernmental Panel on Climate Change (IPCC) Third and Fourth Assessment Reports (often called TAR and AR4, respectively) [Penner *et al.*, 2001; Ramaswamy *et al.*, 2001; Forster *et al.*, 2007]. Kiehl [2007] found that the magnitude of cooling due to the “aerosol effect” in a set of earlier models that were able to replicate the observed historical global surface warming was highly correlated with the strength of a coupled climate model's transient warming response to well-mixed greenhouse gases. Kiehl further noted that much of the uncertainty in total anthropogenic forcing was due to a threefold range of uncertainty in the aerosol forcing used in the different models. This relationship between the “aerosol effect” and the climate model transient sensitivity to well-mixed greenhouse gas (WMGG) warming was further explored by Knutti [2008], who analyzed the full Climate Model Intercomparison Project Phase 3 (CMIP3; AR4) climate model data set and further noted that because most of those models do not incorporate the aerosol indirect effects, their current agreement with observations may be partly spurious. For the models considered in both the TAR and AR4, the “aerosol effect” was primarily driven by aerosol direct radiative effects, with, in some

<sup>1</sup>NOAA Geophysical Fluid Dynamics Laboratory, Princeton, New Jersey, USA.

<sup>2</sup>UCAR/NOAA Geophysical Fluid Dynamics Laboratory, Princeton, New Jersey, USA.

Corresponding author: L. W. Horowitz, NOAA Geophysical Fluid Dynamics Laboratory, Princeton, NJ 08540, USA. (Larry.Horowitz@noaa.gov)

©2013. American Geophysical Union. All Rights Reserved.  
2169-897X/13/10.1002/jgrd.50192

cases, a restricted aerosol indirect effect [Knutti, 2008]. Hansen et al. [2011] recently argued for a large current aerosol climate forcing of  $-1.6 \pm 0.3 \text{ W m}^{-2}$ , whereas Le Treut [2012] summarized recent attempts, via observation, theory, and model, to narrow the possible range for the “aerosol effect.”

[4] Pre-2008 work on the potential role for aerosols in climate change was summarized in the introduction of Levy et al. [2008] and in the references contained therein. More recently, several authors have addressed the nature of the aerosol-cloud interactions [Small et al., 2009; Costantino and Bréon, 2010], the impacts of aerosol emissions on global and regional climate [Shindell and Faluvegi, 2009; Shindell et al., 2009; Koch et al., 2009; Ming and Ramaswamy, 2009; Liao et al., 2009; Wang et al., 2009; Kloster et al., 2010; Shindell et al., 2010; Andrews et al., 2010; Ming et al., 2010; Ming and Ramaswamy, 2011; Ming et al., 2011; Bollasina et al., 2011; Shindell et al., 2012] and precipitation extremes [Chen et al., 2010a], and the role of aerosol indirect effects in climate [Chen et al., 2010b; Quaas et al., 2008].

[5] Levy et al. [2008] used the Geophysical Fluid Dynamics Laboratory’s (GFDL’s) IPCC-AR4 coupled climate model (CM2.1) [Delworth et al., 2006] that was only forced by aerosol direct effects. In that study, CM2.1 used monthly mean concentrations of short-lived radiatively active species that were calculated off-line by a global chemical transport model [Horowitz, 2006] using emissions from the A1B “marker” scenario [Nakicenovic and Swart, 2000]. The study showed that for the A1B-projected increases in BC, OC, and tropospheric ozone and decrease in sulfate aerosols, (1) up to 40% of the simulated summertime surface air warming in the second half of the 21st century, particularly over Northern Hemisphere midlatitude continents, was due to the A1B-projected changes in the short-lived species; (2) the resulting regional patterns of surface temperature warming did not follow the regional patterns of changes in emissions, tropospheric loadings, or direct radiative forcing but were similar to the warming pattern driven by increasing levels of well-mixed greenhouse gases; and (3) there was little significant change in precipitation.

[6] However, this 2008 work included three important caveats: (1) these results only considered direct radiative forcing by aerosols; (2) the emission projections for the short-lived species in the A1B scenario were not well constrained or even necessarily consistent with the scenarios for the well-mixed greenhouse gases, and feedbacks of climate change on short-lived species were neglected; (3) the patterns of regional temperature response, while qualitatively similar among a majority of the suite of AR4 models, were expected to be model dependent, so the results presented from a single model were not necessarily robust.

[7] In this current study, we address Caveat 1 with GFDL’s new fully coupled chemistry-climate model [Donner et al., 2011] with an “aerosol effect” composed of an explicit physical representation of the liquid cloud aerosol indirect effects (cloud droplet activation) and an aerosol direct radiative effect whose calculation assumes an internal mixture of sulfate and BC. Caveat 2 is addressed by calculating aerosol concentrations using the self-consistent emission projections from Representative Concentration Pathway (RCP) 4.5 [Clarke et al., 2007; Smith and Wigley, 2006; Wise et al., 2009; Thomson et al., 2011] within a coupled chemistry-climate model that permits a wide range of climate-chemistry feedbacks.

By comparing the results of this study with our previous one, we partially address Caveat 3, although this study does not consider the role of model resolution and does not span the full range of climate model responses.

[8] Our article is organized as follows: we provide brief descriptions of the coupled climate model, its online chemistry, the model’s treatment of aerosol-water cloud interactions (aerosol indirect effects), and the emissions used in section 2, all of which are described in greater detail elsewhere. The experimental design is discussed in section 3. The role of aerosols during the historical period is discussed in section 4. We then focus on the future projection (RCP4.5) in section 5, where the future impacts of aerosols on temperature and precipitation are presented and analyzed and their implications are then discussed. We summarize our conclusions, identify those that appear to be robust, and address any remaining caveats in section 6.

## 2. Model Description

[9] The new GFDL coupled chemistry-climate model CM3 [Donner et al., 2011; L.W. Horowitz et al., Historical and projected future climate simulated by GFDL CM3 coupled model, in preparation, hereinafter Horowitz et al., 2013] is built on the base of GFDL’s previous coupled climate model (CM2.1) [Delworth et al., 2006], which was used in our earlier study of aerosol impacts on future climate [Levy et al., 2008]. The ocean and sea-ice components in CM3 are essentially unchanged [Griffies et al., 2011]. The important modifications in the coupled model were made in the atmospheric component [for a detailed discussion of these changes, see Donner et al., 2011].

### 2.1. A Summary of New Model Developments in CM3

[10] Rather than specifying cloud-drop number over land ( $300 \text{ cm}^{-3}$ ) and ocean ( $100 \text{ cm}^{-3}$ ) as in CM2.1, a physically realistic and explicit aerosol activation of cloud droplets, requiring subgrid vertical velocities for warm clouds, is used. This work is discussed by Donner et al. [2011] (sections 3d and 3f) and Golaz et al. [2011] and will be summarized in section 2.2.

[11] Although the concentrations of long-lived greenhouse gases and methane are still specified, the distributions of tropospheric and stratospheric ozone and short-lived aerosols are calculated from a fully coupled stratosphere-troposphere chemistry scheme involving merged modules of Horowitz et al. [2003] in the troposphere and Austin and Wilson [2006] in the stratosphere. The chemistry is driven by emissions of the short-lived species and their precursors. In this way, the distribution of the short-lived species and the physical climate are self-consistent. See sections 3f and 3g of Donner et al. [2011] for a summary and Naik et al., Impact of preindustrial to present-day changes in short-lived pollutant emissions on atmospheric composition and climate forcing, submitted to *Journal of Geophysical Research* (hereinafter referred to as Naik et al. [2012]), for a detailed discussion.

[12] The parameterizations of boundary layer and large-scale clouds are the same as in CM2.1. Shallow convection is treated as by Bretherton et al. [2004], and deep convection uses a reduced version of the methods detailed by Donner [1993]. This is summarized in detail in sections 3c, 3d, and 3e of Donner et al. [2011].

[13] The land model in CM2.1 that used specified vegetation and a single bucket hydrology was replaced with a complex land model that includes dynamic vegetation with land use and succession and a multilevel soil hydrology. This work is described by *Shevliakova et al.* [2009] and in Appendix A of *Donner et al.* [2011].

[14] The atmospheric dynamical core was changed to a cubed-sphere formulation [*Putman and Lin, 2007*] with a relatively uniform horizontal grid varying from 163 to 231 km over the globe. The 48 vertical levels range in thickness from 70 m at the surface to 1–1.5 km in the upper troposphere to 2–3 km in most of the stratosphere with a top level at 1 Pa (~86 km). For specific details relevant to CM3, see section 2 of *Donner et al.* [2011].

## 2.2. Aerosol Effects

[15] The “aerosol effect” may be separated into the aerosol direct (radiative) effect [e.g., *Ming et al., 2005*] and all of the aerosol-cloud interactions [e.g., *Lohmann et al., 2010*], which together comprise aerosol indirect effects. Although there are uncertainties associated with the calculation of aerosol direct effects, the magnitude of the aerosol indirect effect is extremely uncertain (see Figures 2.14 and 2.20 in *Forster et al.* [2007]). Reducing this uncertainty is critical to accurately reproducing the historical warming trend for the right reasons and, more importantly, realistically projecting future climate. A key feature of the CM3 model physics is that it simulates aerosol-cloud interactions for liquid clouds [*Ming et al., 2006; Ming et al., 2007; Golaz et al., 2011*], where aerosols act as cloud condensation nuclei (CCN). The larger the number of CCN, the higher the resulting cloud albedo (first indirect effect) and the lower the precipitation efficiency (second indirect effect, sometimes called “cloud lifetime effect”).

[16] Aerosol physical and optical properties are discussed in detail in section 3a.4 of *Donner et al.* [2011]. Sulfate, BC, OC, sea salt, and dust are all considered, although no explicit anthropogenic source of dust is included. A lognormal size distribution is assumed for sulfate, BC, and OC aerosols. The mass size distributions of dust and sea salt are treated with five bins from 0.1 to 10  $\mu\text{m}$ . Hygroscopic growth is considered for sulfate, sea salt, and aged (hydrophilic) black and OC. For the radiative transfer calculation, we assumed an internal mixture of sulfate and aged (hydrophilic) BC that is calculated by a volume-weighted average of their refractive indices. All other aerosols are assumed to be externally mixed. *Donner et al.* [2011] showed (in their Figures 3–5) that aerosol optical depth (AOD), co-albedo, and clear-sky shortwave surface fluxes in CM3 agree better with observations than did the corresponding fields from CM2.1.

[17] The water-soluble aerosols sulfate, sea salt, and organic aerosols are all allowed to be activated into cloud droplets following a physically based parameterization of CCN activation [*Ming et al., 2006*]. Inorganic salts (i.e., sulfate and sea salt) are much more efficient CCN (having higher solubilities and van’t Hoff factors) than organics. Because sea salt, a natural aerosol, does not change appreciably over time, anthropogenic sulfate is the main driver of the changes in CCN abundance over time in CCN and thus of the forcing due to the aerosol indirect effect (as will be demonstrated in sections 4.1–4.2). The grid-mean droplet number concentration is tracked explicitly as part of the prognostic large-scale

cloud scheme [*Ming et al., 2007*]. *Donner et al.* [2011] showed (in their Figure 6) that cloud-drop radii simulated by CM3 capture general patterns retrieved by the Moderate Resolution Imaging Spectroradiometer, with a bias toward smaller droplet sizes. For specific details, see section 3.f in *Donner et al.* [2011].

## 2.3. Emissions

[18] Detailed discussions of the concentrations and emissions used in the historical portion of this study are given in section 2.3 of *Naik et al.* [2012]. They, along with the RCP4.5 scenario, are briefly summarized in the following sections.

[19] Well-mixed greenhouse gas global average concentrations including carbon dioxide ( $\text{CO}_2$ ), nitrous oxide ( $\text{N}_2\text{O}$ ), methane ( $\text{CH}_4$ ), and halocarbons (CFC-11, CFC-12, CFC-113,  $\text{CCl}_4$ ,  $\text{CH}_3\text{Cl}$ ,  $\text{CH}_3\text{CCl}_3$ , HCFC-22,  $\text{Cl}_2$ , and  $\text{Br}_2$ ) are specified from the RCP database developed for climate model simulations for the CMIP5 in support of the IPCC Fifth Assessment Report (AR5) [*Meinshausen et al., 2011*]. Global mean surface concentrations of  $\text{CH}_4$  and  $\text{N}_2\text{O}$  and emissions of short-lived chemical species during the historical period (1860–2005) are from the new emissions data set of *Lamarque et al.* [2010], developed for chemistry-climate model simulations for CMIP5 in support of IPCC-AR5. The inventory provides monthly mean emissions of aerosol species and ozone and aerosol precursors for each decade beginning in 1860. Surface emissions of short-lived reactive chemical species for the period 2005–2100 were provided by RCP4.5 [*Clarke et al., 2007; Thomson et al., 2011; Lamarque et al., 2011*]. In RCP4.5, the short-lived emissions are consistent with one another and with the assumptions that drive the concentrations of the well-mixed greenhouse gases. Natural emissions of dust, sea salt, dimethyl sulfide (DMS), and oceanic primary organic aerosols are calculated interactively as a function of model meteorology and do not show significant trends throughout the historical and future simulations presented here.

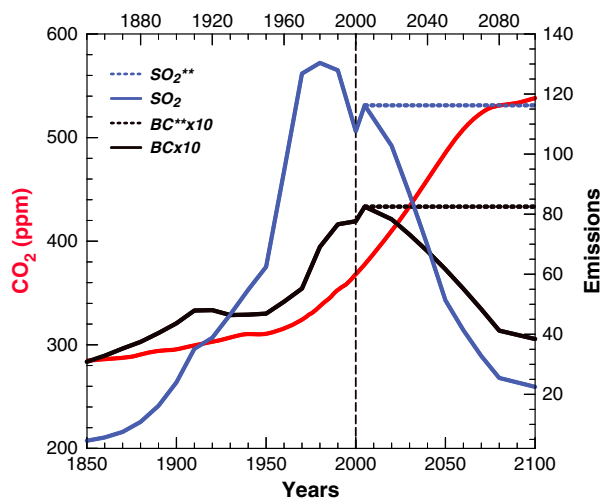


**Figure 1.** Historical and RCP4.5 emissions for  $\text{SO}_2$  (blue) in  $\text{Tg a}^{-1}$  and BC (black) in  $\text{TgC a}^{-1}$  (multiplied by a factor of ten for convenience of plotting) and  $\text{CO}_2$  (red) concentrations in ppmv.

[20] The historical and projected concentrations for CO<sub>2</sub> and the emissions of gaseous SO<sub>2</sub> (precursor of sulfate aerosol) and BC aerosol are shown in Figure 1. The concentrations of CO<sub>2</sub> have been well measured since the late 1950s [Keeling, 1960], and the preindustrial level is well known from ice core data [e.g., Neftel *et al.*, 1985]. The preindustrial level of SO<sub>2</sub> emissions, based on the identified anthropogenic sources, is known to be very small. The question of preindustrial biomass and biofuel sources of BC is far more complex [Lamarque *et al.*, 2010]. According to the current best estimates developed for CMIP5/IPCC-AR5, emissions of SO<sub>2</sub> have grown from a preindustrial level of ~3 TgS a<sup>-1</sup> to the current level of ~55 TgS a<sup>-1</sup>, emissions of BC aerosol from ~3 TgC a<sup>-1</sup> to a current level of ~8 TgC a<sup>-1</sup>, and primary emissions plus secondary production of OC from 93 TgC a<sup>-1</sup> to 113 TgC a<sup>-1</sup> [Lamarque *et al.*, 2010; Naik *et al.*, 2012 and references therein]. By 2100, RCP4.5 projects an 80% reduction in SO<sub>2</sub> emissions, a 50% reduction in BC emissions, and a 35% reduction in OC emissions [Lamarque *et al.*, 2011].

### 3. Experimental Design

[21] The goal of this set of experiments is to use our new coupled chemistry-climate model (CM3) to explore the robustness of our previous finding by Levy *et al.* [2008] that future changes in aerosols may play an important role in 21st century climate change. We examine the key issues that we raised as caveats in Levy *et al.* [2008]: the contribution of aerosol indirect effects, the impact of using a set of self-consistent emission projection, the importance of a self-consistent coupling of atmospheric chemistry and physical climate, and the model dependence of regional patterns of climate response.

#### 3.1. Historical

[22] First, we examine the climate impact of anthropogenic aerosols during the historical period (1860–2005). A three-member ensemble is integrated during this period forced only by the historical changes in anthropogenic emissions of aerosols and their precursors. All other climate forcings, both natural and anthropogenic, are held at 1860 levels for the integration. In particular, global mean concentrations of WMGGs, emissions of ozone precursors, land use, volcanic aerosols, and solar insolation are held constant at 1860 values. Natural emissions of aerosols and aerosol precursors are calculated interactively as a function of model meteorology and so vary from year to year but show little trend over the simulations presented here. The historical emissions for SO<sub>2</sub> (blue) and BC (black) are shown in Figure 1. Although the historical anthropogenic emissions of OC are also included in this study, OC plays a modest role as a forcing agent in CM3 (see section 4.1). This three-member ensemble provides CM3's climate response to its total aerosol effect for the period (1860–2005).

[23] A second three-member ensemble is integrated with the same historical forcing as the first, but with only the aerosol activation into cloud droplets (aerosol indirect effect) seeing the changing aerosol levels. The radiation code in these experiments sees the 1860 aerosol levels (monthly mean climatological concentrations from years 1 to 20 of an 1860 control simulation) throughout the integration, thereby producing no aerosol direct forcing. This second three-member

ensemble thus isolates that fraction of CM3's historical climate response that was solely due to aerosol indirect effects.

[24] We diagnose the radiative forcing provided by aerosol changes in CM3 using an additional set of prescribed sea-surface temperature (SST) simulations with AM3, the atmospheric component of CM3. In these simulations, described in more detail by Horowitz *et al.* [2013], SST and sea ice concentration are prescribed using the AMIP SST and sea ice boundary condition data set [Taylor *et al.*, 2000] prepared for CMIP5. Ensembles of AM3 runs are conducted using (1) fixed 1860 forcing agents, (2) transient anthropogenic and biomass burning emissions of aerosols and aerosol precursors (as used in the historical coupled model integrations), with all other forcing agents fixed at 1860 values, and (3) transient anthropogenic and biomass burning emissions of a single aerosol or aerosol precursor species (BC, OC, or SO<sub>2</sub>, precursor of sulfate), with all other forcing agents (including emissions of other aerosol species) fixed at 1860 values. The change in global mean net radiative flux at the top of the atmosphere in these simulations provides the radiative flux perturbation (RFP) [e.g., Lohmann *et al.*, 2010], also known as the fixed-SST forcing, due to all aerosols ((2)-(1)), or a particular aerosol species ((3)-(1)). In addition, surface RFP (defined as the net radiative flux changes at the surface), which has been linked to changes in precipitation [e.g., Ramanathan *et al.*, 2001], is quantified.

#### 3.2. Projected 21st Century

[25] We use the projections of anthropogenic and biomass burning emissions of short-lived species and long-lived greenhouse gas concentrations from the medium-low forcing RCP4.5 scenario [Clarke *et al.*, 2007; Smith and Wigley, 2006; Wise *et al.*, 2009; Thomson *et al.*, 2011] to examine the climate response of CM3 to projected future levels of anthropogenic aerosols. There are no explosive volcanic eruptions. Two three-member CM3 ensembles are computed, with initial states provided from the end of historical simulations of CM3 with time variation of all forcing agents (anthropogenic and natural). The first ensemble is integrated from 2006 to 2100 and forced by the RCP4.5 projections for all species. The red line in Figure 1 shows the RCP4.5-projected growth of CO<sub>2</sub> from a present-day level of 380 ppmv to a maximum of ~550 ppmv in year 2100. The SO<sub>2</sub> emissions (blue line) decrease sharply by more than 80%, and the BC emissions (black line) decrease by 50%. OC emissions, not shown, decreased by 45% [Naik *et al.*, 2012]. Although the projected CO<sub>2</sub> concentrations and SO<sub>2</sub> emissions in RCP4.5 and A1B are qualitatively similar, they are fundamentally different for BC with a 50% reduction in RCP4.5 and a 100% increase in A1B. We will return to this in section 6, where we compare the CM3 results with the earlier CM2.1 conclusions that were based on A1B projections and only considered the direct radiative effect of aerosols.

[26] A second three-member ensemble, denoted as RCP4.5\*\*, is integrated from 2006 to 2100 and again forced by the same RCP4.5 projection of well-mixed greenhouse concentrations and emissions of ozone precursors. However, the anthropogenic and biomass burning emissions of gaseous SO<sub>2</sub> (dashed blue line) and BC (dashed black line) and OC aerosols (not shown) are held at 2005 values throughout the integrations. As in all simulations, natural emissions of aerosols and aerosol precursors are calculated interactively as a function of model meteorology. The

difference between the two three-member ensembles (RCP4.5 – RCP4.5\*\*) represents CM3’s response to future changes in emissions of aerosols and their precursors as projected by RCP4.5.

[27] Although the response to tropospheric ozone changes was included by *Levy et al.* [2008], it was found to be small and almost completely cancelled by the small negative direct forcing from OC. Sulfate and BC aerosols were dominant (Table 1 in *Levy et al.* [2008]). In this CM3 study with RCP4.5, the tropospheric ozone loading decreases by 8% during the 21st century and plays an even smaller role. We focus here specifically on the role of anthropogenic aerosols. Both the OC and BC atmospheric loadings return to near their preindustrial levels by 2100

[28] As for the historical simulations, the radiative forcing from aerosols in the RCP4.5 scenario is diagnosed using a set of prescribed SST simulations with AM3. In this case, climatological SST and sea ice for 1981–2000 from the HadISST data set [*Rayner et al.*, 2003] were used. Simulations of AM3 are conducted using (1) fixed 1860 forcing agents and (2) transient anthropogenic and biomass burning emissions of aerosols and aerosol precursors (as used in the coupled model RCP4.5 integrations), with all other forcing agents fixed at 1860 values. The change in global mean net radiative flux at the top of the atmosphere in these simulations ((2)-(1)) provide the RFP due to all aerosols.

#### 4. Historical Impacts of Aerosols

[29] Before exploring the potential contributions of aerosols to 21st century climate, it is useful to consider their role during the historical period where we have observations of surface temperature, precipitation, and most of the well-mixed greenhouse gases, as well as recent measurements of the two key aerosols, sulfate and BC, reasonable estimates of early anthropogenic sulfate aerosol levels, and less certain but at least plausible estimates of early levels of BC.

#### 4.1. AOD and Aerosol RFP

[30] During the historical period, in the three-member ensemble of CM3 forced solely by historical anthropogenic and biomass burning emissions of BC, OC and SO<sub>2</sub> (Figure 1) with all other forcing agents held constant at 1860 levels, AOD increases by approximately 40% (Table 1). A majority of the AOD increase is attributed to sulfate aerosol, with sulfate burden (not shown, see *Naik et al.* [2012]) and sulfate optical depth (Table 1) following a similar time evolution as total AOD, with sulfate optical depth increasing from approximately 0.02 in 1860 and reaching 0.03 by around 1920, 0.04 by 1955, and 0.06 by 1980.

[31] Radiative forcing calculations [*Horowitz et al.*, 2013], introduced in section 3.1, show that the top-of-atmosphere RFP (Table 1) resulting from changes in all aerosol and aerosol precursor emissions is  $-1.78 \text{ W m}^{-2}$  (for 1996–2005 emissions versus 1860 emissions). The corresponding RFP resulting from changes in SO<sub>2</sub> emissions (precursor of sulfate aerosol) alone is  $-1.74 \text{ W m}^{-2}$ , whereas those for BC and OC emission changes during the same period are  $+0.13$  and  $-0.38 \text{ W m}^{-2}$ , respectively.

[32] The sum of the individual species RFPs (sulfate + BC + OC) exceeds in magnitude the total aerosol RFP, indicating a nonlinearity in the aerosol RFPs. Essentially, this likely results from OC causing a significant indirect effect in the absence of anthropogenic sulfate aerosol, but having little additional indirect effect in an atmosphere containing anthropogenic sulfate.

[33] The RFP for all aerosol and aerosol precursor emissions (Table 1) is more strongly negative at the surface ( $-2.9 \text{ W m}^{-2}$ ) than at the top of atmosphere ( $-1.78 \text{ W m}^{-2}$ ). Emissions of SO<sub>2</sub> provide the greatest contribution to the negative surface RFP ( $-2.1 \text{ W m}^{-2}$ ), followed by smaller values from emissions of BC ( $-0.5 \text{ W m}^{-2}$ ) and OC ( $-0.4 \text{ W m}^{-2}$ ).

#### 4.2. Global Mean Surface Temperature

[34] Figure 2 shows the global mean surface air temperature resulting from the three-member ensemble of CM3 forced by

**Table 1.** Global Mean AOD, Absorption AOD, Sulfate AOD, Surface Air Temperature, Precipitation, and Aerosol RFP

	1860 <sup>a</sup>	2000 <sup>b</sup>	2100 <sup>c,f</sup>		
			RCP4.5	RCP4.5	RCP4.5**
AOD	0.1015	0.1440	0.1572	0.1222	0.1626
Absorption AOD	0.0043	0.0072	0.0079	0.0059	0.0084
Sulfate AOD	0.0215	0.0556	0.0657	0.0367	0.0688
Surface air temperature (K) <sup>g</sup>	286.9	285.9	287.5	289.7	288.8
Precipitation (mm day <sup>-1</sup> )	3.03	2.95	3.02	3.17	3.08
Aerosol RFP (W m <sup>-2</sup> ) <sup>h</sup>	N/A	-1.78 (-2.9)	-1.75 (-2.9)	-0.49 (-0.9)	
Sulfate RFP (W m <sup>-2</sup> ) <sup>h</sup>	N/A	-1.74 (-2.1)	-1.66 (-2.1)	-0.61 (-0.6)	
BC RFP (W m <sup>-2</sup> ) <sup>h</sup>	N/A	+0.13 (-0.5)	+0.03 (-0.6)	-0.02 (-0.2)	
OC RFP (W m <sup>-2</sup> ) <sup>h</sup>	N/A	-0.38 (-0.4)	-0.27 (-0.4)	-0.02 (-0.0)	

<sup>a</sup>Mean values for years 1–200 of the 1860 control simulation of CM3.

<sup>b</sup>Mean values for years 1996–2005 for the three-member ensemble of CM3 simulations with time-varying aerosol and aerosol precursor emissions (all other forcings held at 1860 values). Note that these values differ from those that would be obtained from CM3 simulations including time variation of all forcing agents.

<sup>c</sup>Mean values for years 2006–2015 for the three-member ensemble of CM3 simulations forced by RCP4.5 (for all forcing agents).

<sup>d</sup>Mean values for years 2091–2100 for the three-member ensemble of CM3 simulations forced by RCP4.5 (for all forcing agents).

<sup>e</sup>Mean values for years 2091–2100 for the three-member ensemble of CM3 simulations forced by RCP4.5\*\* (with aerosol and aerosol precursors held at year 2005 values, but all other forcing agents following RCP4.5).

<sup>f</sup>Note that the RCP4.5/RCP4.5\*\* simulations are initialized in year 2006 from the end of historical simulations, including time variation of all forcing agents, and thus have a different present-day state from the historical aerosol-only simulations.

<sup>g</sup>Global mean surface air temperatures have been adjusted by subtracting the long-term drift ( $0.001 \text{ }^\circ\text{C a}^{-1}$ ) in the 1860 control simulation of CM3.

<sup>h</sup>RFP is calculated as the net radiative flux change at the top of the atmosphere in prescribed SST simulations with time-varying versus 1860 aerosol and aerosol precursor emissions, as described in sections 3.1–3.2. Values in parentheses are RFP at the surface.

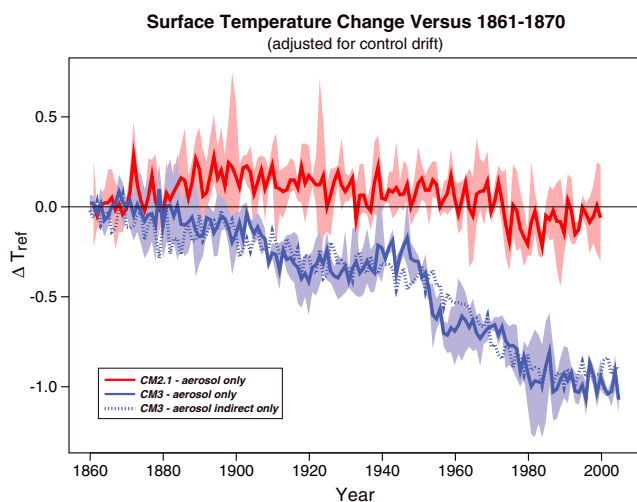


**Figure 2.** Historical change in global mean surface air temperature (at 2 m) simulated by CM2.1 (red shading for three-member ensemble envelope and red line for ensemble mean) and CM3 (blue shading for three-member ensemble envelope and blue line for ensemble mean). Both models are forced by changing concentrations (CM2.1) or emissions (CM3) of sulfate ( $\text{SO}_2$  emissions in CM3), BC, and OC aerosols whereas all other forcing agents, natural and anthropogenic, are held fixed at 1860 (or 1861 for CM2.1) values. In the case of CM2.1, natural aerosol concentrations (dust, sea salt) are held constant; whereas in CM3, their emissions are calculated interactively. Also shown (dashed blue line) is mean surface air temperature change from a three-member CM3 ensemble in which aerosol emission changes affected only aerosol activation into cloud droplets (aerosol indirect effect), whereas the radiation code (aerosol direct effect) used climatological 1860 aerosol abundances. All temperature changes were adjusted for drift in corresponding 1860 control simulations. See section 3.1 for details of model simulations.

historical emissions of BC, OC, and  $\text{SO}_2$  with all other forcing agents, natural and anthropogenic, held constant at 1860 levels. For the historical period, aerosol and aerosol precursor emission changes result in  $1.0^\circ\text{C}$  of global cooling, with two thirds of the cooling occurring after 1940 and a leveling off in the 1980s, just as  $\text{SO}_2$  emissions reach their maximum (see Figure 1). The temperature response from the second three-member ensemble integration where only the aerosol activation into cloud water droplets (aerosol indirect effects) sees the changing aerosols is shown by the dashed blue line in Figure 2. Although both time series are quite noisy, there is no statistically significant difference between the solid and dashed blue lines during the historical period, demonstrating that the aerosol cooling effect in CM3 results essentially from the aerosol indirect effect.

[35] To summarize, during the historical period, the total aerosol effect in CM3 results essentially from the aerosol indirect effect, with the net direct effect (difference between solid and dashed blue lines in Figure 2) being near zero. The near-zero direct effect is a consequence of aerosol-induced atmospheric absorption by BC being offset to a large extent by OC and sulfate scattering. Although the direct effect causes little change in surface temperature, it does have a

significant role in the hydrological cycle as explained in section 5.3. The aerosol indirect effect is dominated by changes in sulfate aerosol, as indicated by the large sulfate RFP nearly matching the total aerosol RFP. The influence of sulfate on surface temperatures in CM3 has been confirmed by two additional sets of simulations, in which only  $\text{SO}_2$  emissions or only BC emissions are allowed to evolve in time, with all other forcing agents held constant at 1860 values. These additional simulations result in  $-1.1^\circ\text{C}$  of cooling at 1996–2005 in response to  $\text{SO}_2$  emission changes (nearly identical to the result of  $-1.0^\circ\text{C}$  from the simulation with all aerosol and aerosol precursor emissions changing), with no significant surface temperature change resulting from historical changes in BC emissions.

[36] In Figure 2, we also compare the very different global mean surface temperature responses of CM3, forced by historical aerosol emissions, and our earlier climate model, CM2.1, forced only by the aerosol direct effect using specified sulfate, BC, and OC aerosol concentrations [see Schwarzkopf and Ramaswamy, 2008 for CM2.1 experimental design]. Early in the historical record, CM2.1 shows modest warming ( $0.1$ – $0.2^\circ\text{C}$ ), due to increasing BC, that is followed by a modest cooling after sulfate aerosol starts increasing strongly (for the sulfate and BC time series, see Figure 2 of Horowitz [2006]). By 2000, the net aerosol direct effect on CM2.1's global surface temperature is at most  $-0.1^\circ\text{C}$  of cooling. This is a result of the strong BC absorption (warming) almost canceling the strong sulfate scattering (cooling). CM2.1's very weak net aerosol direct effect is comparable with the aerosol direct effect in CM3 where the more modest historical increase in BC [Naik et al., 2012] is balanced by our assumption in CM3 that BC and sulfate are internally, not externally, mixed. CM3's much larger total aerosol effect ( $1.0^\circ\text{C}$  of surface cooling by 2005) is the result of the model's strong aerosol indirect effect, along with the near cancellation of its OC, BC, and sulfate direct effects.

#### 4.3. Global Mean Precipitation

[37] In Figure 3, we examine the CM3 historical response of global mean precipitation to anthropogenic aerosol forcing and compare it with the response to anthropogenic aerosols in CM2.1, which again is driven only by the aerosol direct effect. Although both models show a significant reduction in global precipitation, the reduction in CM3 is three times the reduction in CM2.1. Both CM2.1 and CM3 (difference between solid and dashed blue lines) show a similar 1% reduction in global mean precipitation during the historical period when forced by only the aerosol direct effect, although neither simulation shows significant global mean surface cooling. Unlike the CM3 response for global mean temperature (which is almost entirely due to the aerosol indirect effect), only two thirds of the precipitation response is due to the aerosol indirect effect (dashed blue line). Both large-scale and convective precipitation in CM3 are reduced in response to aerosols, with somewhat larger percent reductions in large-scale ( $-3.7\%$  for total aerosol effect,  $-2.9\%$  for indirect effect) versus convective precipitation ( $-2.9\%$  and  $-1.5\%$ , respectively).

[38] We can explain the global mean precipitation change by considering the atmospheric energy balance. The atmospheric longwave cooling is primarily balanced by latent heating,

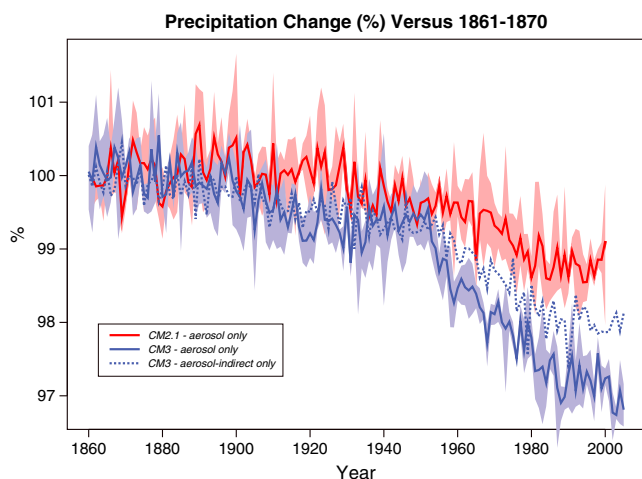


**Figure 3.** Global mean percentage precipitation change relative to (1861–1870) average simulated by CM2.1 (red shading for three-member ensemble envelope and red line for ensemble mean) and CM3 (blue shading for three-member ensemble envelope, blue line for ensemble mean, blue dashed line for three-member mean when only forced by aerosol indirect effects). Both models are forced by changing levels of sulfate, BC, and OC aerosols (emissions for CM3, concentrations for CM2.1), whereas all other forcing agents, natural and anthropogenic, are held fixed at 1860 (or 1861 for CM2.1) values. In the case of CM2.1, natural aerosol concentrations (dust, sea salt) are held constant, whereas in CM3 their emissions are calculated interactively. See text for details.

for which precipitation is a good proxy, and by atmospheric absorption. *Ming et al.* [2010] argued that aerosols alter the global mean precipitation in two ways. First, they decrease surface temperature, leading to a cooler troposphere. In turn, the cooler troposphere experiences less longwave cooling [*Allen and Ingram, 2002*], thus requiring reduced latent heating and precipitation to maintain energy balance. Second, absorbing aerosols (mainly BC) directly heat the atmosphere, offsetting a portion of the longwave cooling, thus also reducing condensation heating and precipitation. Both factors contribute to the drying present in CM2.1 and CM3. The first effect (decreased surface temperature) explains why the global mean precipitation reduction is much smaller in CM2.1 than in CM3, owing to the much smaller surface cooling in CM2.1. The second effect (increased atmospheric absorption) is the primary source of drying in CM2.1 and may partly explain the difference between the CM3 aerosol indirect-only effect and the full aerosol effect, which includes enhanced absorption by carbonaceous aerosols and therefore increased drying.

## 5. Impact of Aerosols on the 21st Century Climate

[39] Before examining the CM3 response to projected 21st century (RCP4.5) decreases in BC and SO<sub>2</sub> emissions, we should address the fact that CM2.1, which had a very modest global mean surface cooling in response to the historical increase in BC and sulfate (Figure 2), showed a strong warming in the second half of the 21st century in response to the projected aerosol emissions in A1B [*Levy*

*et al.*, 2008]. This strong aerosol response predicted by CM2.1 for the 21st century was due to the A1B projection of increasing BC and decreasing sulfate aerosols, both of which produced significant positive radiative forcings and therefore led to a significant net warming. Given that the newer set of RCP projections all have decreases in both BC and sulfate aerosols, the second caveat regarding emission projection inconsistencies was clearly justified in the 2008 paper. As we will see, so was the first caveat regarding the potential role of aerosol indirect effects. For the rest of this study, we use RCP4.5, which provides a consistent set of well-mixed greenhouse gas concentrations and short-lived anthropogenic emissions of gases and aerosols [*Clarke et al.*, 2007; *Thomson et al.*, 2011; *Meinshausen et al.*, 2011]. Although nobody can predict the future out to 2100, RCP4.5 treats all of the emissions, both for well-mixed greenhouse gases and for the short-lived species, in a logical and consistent manner and makes credible assumptions about the relatively distant future.

### 5.1. AOD and Aerosol RFP

[40] Following the RCP4.5 scenario, aerosol and aerosol precursor emissions decrease sharply during the 21st century (Figure 1). As a result, AOD in CM3 decreases by approximately 25%, and sulfate burden (not shown) and sulfate AOD decrease by almost 50% from present day (2006–2015) by the end of the century (2091–2100; Table 1). Absorption AOD (primarily from BC) decreases by approximately 25%. In the RCP4.5\*\* simulation, in which aerosol and aerosol precursor emissions are held constant at year 2005 levels, aerosol loadings and AOD are found to increase modestly by approximately 5% during the 21st century, as a result of changes in aerosol lifetime [*Fang et al.*, 2011].

[41] As a result of the decrease in aerosol loading projected by the RCP4.5 scenario, aerosol RFP is dramatically reduced in magnitude, from  $-1.75 \text{ W m}^{-2}$  in (2006–2015) to  $-0.49 \text{ W m}^{-2}$  in (2091–2100), as shown in Table 1. As was the case for the increase in the magnitude of aerosol RFP during the historical period (section 4.1), SO<sub>2</sub> emission changes (and sulfate aerosol abundance changes) dominate the change in aerosol RFP during the 21st century. The surface aerosol RFP also diminishes in response to the decreased aerosol loading, from  $-2.9 \text{ W m}^{-2}$  (2006–2015) to  $-0.9 \text{ W m}^{-2}$  (2091–2100).

### 5.2. Global Mean Surface Temperature

[42] Figure 4 shows the global mean surface temperature response of CM3 following the RCP4.5 scenario and the RCP4.5\*\* scenario (in which BC, OC, and SO<sub>2</sub> emissions are fixed at year 2005 levels). Global mean surface temperatures are projected by CM3 to increase by 2.2 °C during the 21st century (Table 1), with 0.9 °C of that increase (40%) due to the decrease in aerosol and aerosol precursor emissions projected by RCP4.5. The warming due to the full RCP4.5 projection is comparable with that projected by CM2.1 for the A1B scenario, although CO<sub>2</sub> is 150 ppm higher in the A1B scenario by 2100. This is a result of CM3's stronger aerosol effect (aerosol reduction resulting in a warming) and stronger transient climate response [*Winton et al.*, 2012; *Horowitz et al.*, 2013].

[43] The global mean warming resulting from 21st century aerosol changes in CM3 (RCP4.5 – RCP4.5\*\*, 0.9 °C) is

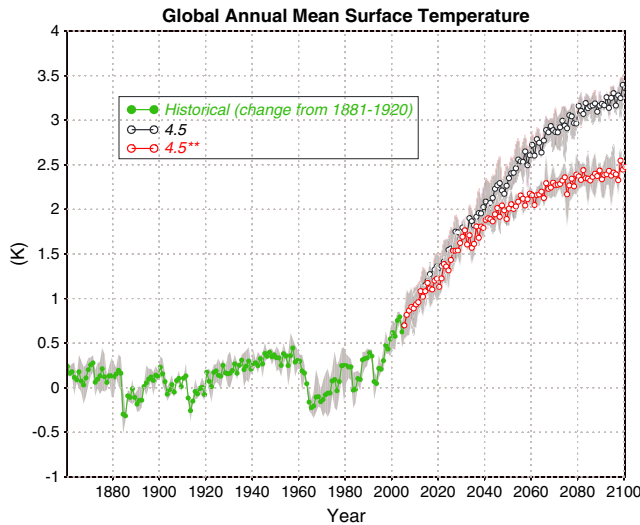


**Figure 4.** Global mean annual surface temperature time series simulated by CM3, which is forced by the historical change in all radiative forcing agents from 1860 until 2005 (gray shading is a five-member ensemble envelope, and green dots are annual means) and then from 2006 to 2100 by either RCP4.5 (gray shading is three-member ensemble envelope, and open black circles are annual means) or by RCP4.5\*\* (BC, OC, and SO<sub>2</sub> emissions held fixed at 2005 values, the gray shading is the three-member ensemble envelope, and the open red circles are annual means). All of the surface temperature data are plotted relative to the 1881–1920 average.

much larger than the comparable warming in CM2.1 (A1B – A1B\*, 0.4 °C). Although this increased response is in part due to significant differences between the present-day distributions of aerosols in the two models and between the A1B and the RCP4.5 projections of future aerosol emission changes, it is likely primarily the result of the strong aerosol indirect effect in CM3 that is missing in CM2.1. The different mixing-state assumptions in CM2.1 (external mixture) and CM3 (internal mixture of sulfate and BC) modify the magnitude of the direct effect, as demonstrated by *Ocko et al.* [2012] for CM2.1.

### 5.3. Global Mean Precipitation

[44] In Figure 5, we show that the warming climate in RCP4.5 enhances global mean precipitation, as expected, by  $\sim 0.15 \text{ mm day}^{-1}$  by 2100. In our earlier study with CM2.1 forced by A1B, global mean precipitation only increased by  $0.05 \text{ mm day}^{-1}$  [see Figure 8b of *Levy et al.*, 2008]. Unlike the earlier CM2.1 results where the changing levels of aerosols (A1B – A1B\*) were found to have no statistically significant impact on precipitation [Figure 8 in *Levy et al.*, 2008], the precipitation differences between the RCP4.5 and the RCP4.5\*\* three-member ensembles show clear statistical separation by 2050. The increase in precipitation in RCP4.5 compared with RCP4.5\*\* can be explained by both a surface temperature warming from the reduction in sulfate aerosols and a diminished atmospheric absorption effect from the reduction in BC, both of which should result in increased condensation heating (precipitation) to maintain energy balance (see discussion in section 4.3). By contrast, in CM2.1, the negligible global mean precipitation

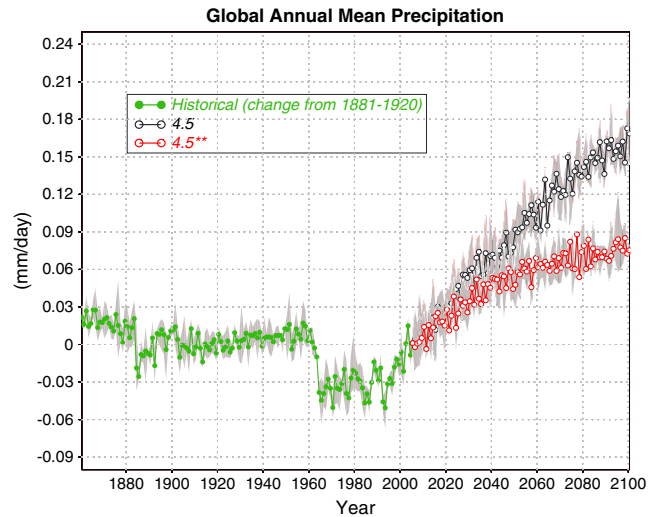


**Figure 5.** Global mean annual precipitation time series simulated by CM3, which is forced by the historical change in all radiative forcing agents from 1860 until 2005 (gray shading is a five-member ensemble envelope, and green dots are annual means) and then from 2006 to 2100 by either RCP4.5 (gray shading is three-member ensemble envelope, and open black circles are annual means) or by RCP4.5\*\* (BC, OC, and SO<sub>2</sub> emissions held fixed at 2005 values, the gray shading is the three-member ensemble envelope, and the open red circles are annual means). All of the precipitation data are plotted relative to the 1881–1920 average.

difference between A1B and A1B\* results from a balance between the increased surface temperature effect on condensation heating (precipitation) and the effect of increased atmospheric BC absorption (decreased condensation heating), as discussed in section 4.3. For further discussion of this topic, see *Ming et al.* [2010].

### 5.4. Regional Surface Temperature

[45] Although the global mean responses are a useful first check of a model’s response, the policy-based questions, not to mention the more challenging scientific assessments, require an examination of regional simulations. In Figure 6a, we subtract the surface temperatures during Northern Hemisphere summertime (June–August) at the end of the 21st century in the RCP4.5\*\* simulations from those for RCP4.5 to determine CM3’s response to the RCP4.5-projected aerosol emission reductions. The colored areas in Figure 6a represent regions where summertime surface temperatures show a statistically significant response (at the 95% confidence level) to projected aerosol changes.

[46] Both the current CM3 figure and the previous CM2.1 summertime temperature response to the A1B projections of changes in short-lived species [see Figure 6f in *Levy et al.*, 2008] show significant warming across much of the Northern Hemisphere with the strongest impacts over central North America, Western Europe including the Mediterranean, and Central Asia. Although CM3’s forced warming is significantly stronger and statistically significant over a wider area, the general regional patterns are similar between the two models. As previously discussed, e.g., in the IPCC-AR4 report [*Randall et al.*, 2007; *Christensen et al.*, 2007], models

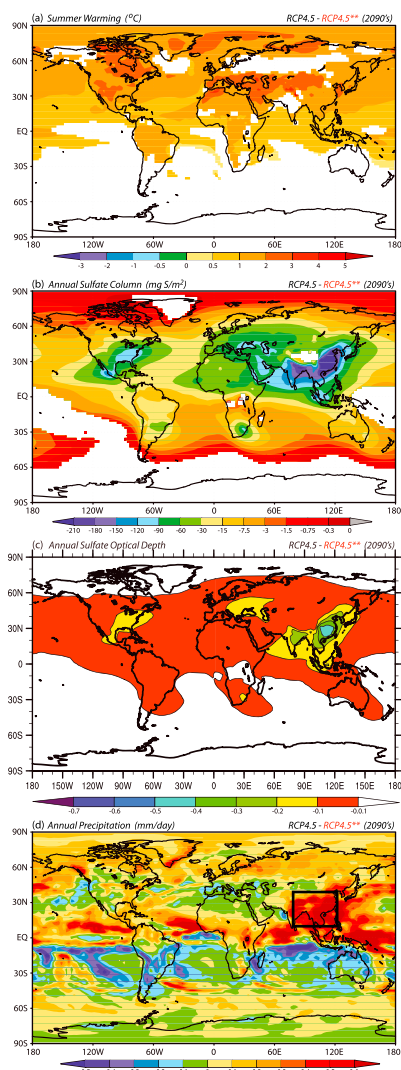


**Figure 6.** (a) Surface air temperature warming ( $^{\circ}\text{C}$ ) during Northern Hemisphere summer (June–August) due to RCP4.5-projected changes in aerosol and aerosol precursor emissions, calculated by subtracting a three-member ensemble simulation of CM3 forced by RCP4.5\*\* from a three-member ensemble simulation of CM3 forced by RCP4.5, both ensembles averaged over 2091–2100. (b) Annual average change in sulfate column ( $\text{mg S m}^{-2}$ ) due to RCP4.5-projected changes in aerosol and aerosol precursor emissions, calculated by subtracting a three-member ensemble simulation of CM3 forced by RCP4.5\*\* from a three-member ensemble simulation of CM3 forced by RCP4.5, both ensembles averaged over 2091–2100. (c) Annual mean change in AOD (at 550 nm) from sulfate aerosols due to RCP4.5-projected changes in aerosol and aerosol precursor emissions, calculated by subtracting a three-member ensemble simulation of CM3 forced by RCP4.5\*\* from a three-member ensemble simulation of CM3 forced by RCP4.5, both ensembles averaged over 2091–2100. (d) Annual mean precipitation change ( $\text{mm day}^{-1}$ ) due to changes in aerosol and aerosol precursor emissions, calculated by subtracting a three-member ensemble simulation of CM3 forced by RCP4.5\*\* from a three-member ensemble simulation of CM3 forced by RCP4.5, both ensembles averaged for 2091–2100.

with  $\sim 200$  km horizontal resolution are not expected to realistically represent subcontinental regional detail. In our CM2.1 study, the strongest U.S. summer response was in the central United States; whereas in CM3, the strongest summer response is in the western United States.

[47] We next compare the CM3 warming due to RCP4.5 aerosol reductions (Figure 6a) with the related distribution of changes in tropospheric sulfate column (Figure 6b) and sulfate optical depth (AOD; Figure 6c) during the 21st century. We focus on sulfate because both calculations of RFP (Table 1) and global mean surface temperature response (Figure 2) show that the aerosol temperature response in CM3 is dominated by sulfate aerosol. The pattern of aerosol RFP (not shown, see *Horowitz et al.* [2013]) is similar to the patterns of sulfate column and sulfate AOD reductions, with maximum positive RFP occurring in regions with large reductions in sulfate. The resulting RFP pattern is similar to the direct forcing pattern found in CM2.1 from the A1B changes in short-lived species, primarily sulfate and BC aerosol [Figure 3b by *Levy et al.*, 2008]. As in the *Levy et al.* [2008] study using CM2.1, there is little pattern correlation between the reduced sulfate column (or sulfate AOD or RFP) and the surface temperature response in CM3. Although A1B and RCP4.5 have many differences, they both agree that the major 21st century changes in aerosols are found over East and South Asia. Similarly, both CM2.1 and CM3 have their strongest surface temperature responses over North America, Western Europe, and parts of Russia, not over South and East Asia.

### 5.5. Regional Precipitation

[48] In Figure 6d, we examine the regional distribution of the CM3 precipitation response to the aerosol reductions projected by RCP4.5 and compare that distribution with the distribution of sulfate column changes in Figure 6b. Unlike the previous case of surface temperature, the maximum precipitation response over land correlates strongly with the reduction in the sulfate column, particularly over South and East Asia. Statistically significant precipitation changes are primarily limited to these regions. Most of the dark red and blue areas outside Asia in Figure 6d are not statistically significant at the 95% confidence level, particularly over the tropical ocean. *Bollasina et al.* [2011] argued that aerosols in CM3 weaken the region’s monsoonal circulation and rainfall by preferentially shielding the Northern Hemisphere from solar heating. Our result that removing aerosols enhances the South and East Asian summertime rainfall in the same model is consistent with that argument. Other studies have identified various mechanisms contributing to the regional response of Indian monsoon precipitation to aerosol forcing in different models, including a larger role for absorbing aerosols [*Wang et al.*, 2009] and anomalous anticyclonic flow around the Indian subcontinent associated with localized sea-level pressure changes [*Shindell et al.*, 2012].

[49] In Figure 7, we focus on the area outlined by the black box in Figure 6d and considered the summertime (June–August) precipitation time series for that region in RCP4.5 and RCP4.5\*\*. Clearly, these two time series, while highly variable, separate by 2050. By 2100, the RCP4.5 global reductions in aerosols lead to an increase in precipitation over East Asia of  $\sim 1$  mm day $^{-1}$ . Interestingly, the  $1.3^{\circ}\text{C}$  of global

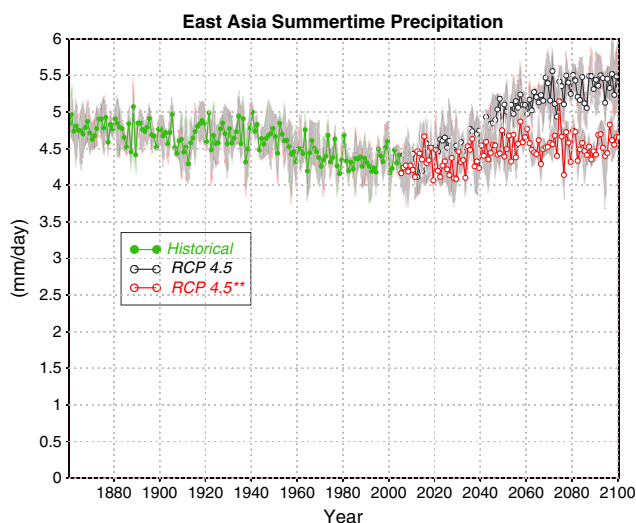


**Figure 7.** Precipitation ( $\text{mm day}^{-1}$ ) simulated by CM3, averaged over the area outlined in the black box in Figure 6d during Northern Hemisphere summer (June–August). CM3 is forced by the historical change in all radiative forcing agents from 1860 until 2005 (gray shading is a five-member ensemble envelope, and green dots are annual means) and then from 2006 to 2100 by either RCP4.5 (gray shading is three-member ensemble envelope, and open blue circles are annual means) or by RCP4.5\*\* (BC, OC, and  $\text{SO}_2$  emissions held fixed at 2005 values, the gray shading is the three-member ensemble envelope and the open red circles are annual means).

warming associated with the RCP4.5\*\* scenario (Figure 4, Table 1) results in a very modest  $\sim 0.2 \text{ mm day}^{-1}$  of increased precipitation over East Asia. This regional CM3 precipitation response is dominated by the reduction in sulfate and BC aerosols.

## 6. Summary and Conclusions

### 6.1. Historical Impact of Aerosols (1860–2005)

[50] 1. For temperature, we find that the total effect of anthropogenic aerosols in CM3 is driven by the aerosol indirect effect, with the net direct effect being near zero and the indirect effect being dominated by changes in sulfate aerosol.

[51] 2. Although CM3 and CM2.1 both have very small global mean surface temperature responses to their net aerosol direct effect ( $\sim 0.1^\circ\text{C}$  or less of cooling), the very strong aerosol indirect effect in CM3 results in  $1.0^\circ\text{C}$  of total cooling from historical changes in aerosol and aerosol precursor emissions by 2005.

[52] 3. The global precipitation decrease in CM3 in response to the large historical increases in anthropogenic aerosols is three times larger than that in CM2.1, again due to the strong aerosol indirect effect in CM3.

### 6.2. Projected 21st Century Impact of Aerosols (2006–2100)

[53] 1. CM3, driven by emission reductions in anthropogenic aerosols and their precursors projected by RCP4.5, produces  $\sim 1^\circ\text{C}$  of additional global mean warming by 2100, more than twice the response in CM2.1 driven by A1B.

[54] 2. As was the case with CM2.1, CM3's highly non-uniform surface warming patterns driven by aerosol forcing are uncorrelated with the spatial distribution of the aerosol column reductions. For temperature, the indirect effect of sulfate is the primary aerosol driver.

[55] 3. In CM3, emission reductions of anthropogenic aerosols and their precursors projected by RCP4.5 produce  $\sim 0.1 \text{ mm day}^{-1}$  of additional precipitation by the end of the 21st century, whereas the previous results for the impact of A1B-projected aerosol changes in CM2.1 showed no statistically significant precipitation response.

[56] 4. Unlike temperature, the largest precipitation increases in CM3 are collocated with the greatest decreases in sulfate aerosols, in and downwind of Asia, where we find precipitation in East and South Asia increasing by  $\sim 1.0 \text{ mm day}^{-1}$  through the second half of the 21st century.

### 6.3. Conclusions

[57] Using the new GFDL chemistry-climate model, CM3, we arrive at the following conclusions:

[58] 1. Projected 21st century aerosol emission changes have even stronger impacts on future temperature and precipitation than previously concluded by *Levy et al.* [2008].

[59] 2. The inclusion of aerosol indirect effects in CM3 greatly enhances the impacts of aerosols on both temperature and precipitation.

[60] 3. The response of surface temperature to aerosols is dominated by sulfate, as demonstrated by RFP calculations and sensitivity simulations in which only  $\text{SO}_2$  emissions vary historically, whereas precipitation responds to both the sulfate-driven temperature effect and the BC-driven atmospheric absorption.

[61] 4. We believe that the RCP4.5 projection, which treats all of the short-lived emissions and well-mixed concentrations in a self-consistent manner, is more credible than the previous A1B scenarios that did not include several critical short-lived species. Nonetheless, there are still important caveats associated with emissions that are discussed in the next section.

### 6.4. Caveats

[62] Caveat 1 from *Levy et al.* [2008] concerned the lack of an aerosol indirect effect in CM2.1. Aerosol indirect effects are critical and must be included in any assessment of aerosol impacts on climate.

[63] Caveat 2 from *Levy et al.* [2008] concerned the lack of a consistent treatment of aerosol and aerosol precursor emissions in A1B. Although the RCP4.5 21st century projections of aerosol and aerosol precursor emissions are still uncertain, they at least used logically consistent assumptions across the projections for both the short-lived species emissions and well-mixed greenhouse gas concentrations.

[64] Caveat 3 from *Levy et al.* [2008] concerned the model dependence of patterns of regional temperature response. Continental-scale patterns seem to be quite robust between CM2.1 and CM3, but model resolution remains an issue for subcontinental regional climate responses.

[65] The current caveats are as follows:

[66] 1. Emissions of BC and OC are still quite uncertain. In particular, the past, present, and future levels of OC are highly uncertain. The good news is that BC and OC tend to cancel each other's direct forcing, and sulfate tends to dominate the indirect effect.

[67] 2. We did not consider nitrate aerosol forcing. Although nitrate aerosol is not likely to have played a significant role up until now, it may grow in importance if sulfate, BC, and OC levels all decline [Bauer et al., 2007; Bellouin et al., 2011].

[68] 3. Although reasonably confident of the strength of our first indirect aerosol effect in CM3, we know that our representation of the second indirect effect (“cloud lifetime effect”) is incomplete and suspect that it and our total aerosol effect are too strong [Ackerman et al., 2004; Quaas et al., 2009; Guo et al., 2011].

## 7. Final Statement

[69] Based on all of the current RCP’s, we conclude that the historical increases in global levels of OC, BC, and sulfate are expected to reverse significantly during the 21st century as the developing economies apply existing pollution control technology to clean up their own air. Whatever atmospheric heating has been currently masked by the rising levels of aerosols will then be exposed.

[70] Until we determine or at least narrow the range of either our estimate of the transient climate response of the earth’s climate to well-mixed greenhouse gases or the associated magnitude of the total “aerosol effect” on the earth’s climate [Kiehl, 2007; Knutti, 2008], we will not be able to credibly narrow the estimated impact of anthropogenic aerosols on climate as well as the overall climate response to projected 21st century anthropogenic emissions of all radiative species.

[71] **Acknowledgments.** The authors appreciate the helpful comments and suggestions from Leo J. Donner and Michael Winton on this article. Comments from two anonymous reviewers were also helpful in improving the manuscript.

## References

- Ackerman, A. S., M. P. Kirkpatrick, D. E. Stevens, and O. B. Toon (2004), The impact of humidity above stratiform clouds on indirect aerosol climate forcing, *Nature*, *432*, 1014–1017.
- Allen, M. R., and W. J. Ingram (2002), Constraints on future changes in climate and the hydrologic cycle, *Nature*, *419*, 224–232.
- Andrews, T., P. M. Forster, O. Boucher, N. Bellouin, and A. Jones (2010), Precipitation, radiative forcing and global temperature change, *Geophys. Res. Lett.*, *37*, L14701, doi:10.1029/2010GL043991.
- Austin, J., and R. J. Wilson (2006), Ensemble simulations of the decline and recovery of stratospheric ozone, *J. Geophys. Res.*, *111*, D16314, doi:10.1029/2005JD006907.
- Bauer, S. E., D. Koch, N. Unger, S. M. Metzger, D. T. Shindell, and D. G. Streets (2007), Nitrate aerosols today and in 2030: Importance relative to other aerosol species and tropospheric ozone, *Atmos. Chem. Phys.*, *7*, 5043–5059, doi:10.5194/acp-7-5043-2007.
- Bellouin, N., J. Rae, A. Jones, C. Johnson, J. Haywood, and O. Boucher (2011), Aerosol forcing in the Climate Model Intercomparison Project (CMIP5) simulations by HadGEM2-ES and the role of ammonium nitrate, *J. Geophys. Res.*, *116*, doi:10.1029/2011JD016074.
- Bollasina, M. A., Y. Ming, and V. Ramaswamy (2011), Anthropogenic Aerosols and the Weakening of the South Asian Monsoon, *Science*, doi:10.1126/science.1204994.
- Bretherton, C. S., J. R. McCaa, and H. Grenier (2004), A new parameterization for shallow cumulus convection and its application to marine subtropical cloud-topped boundary layers. Part I: Description and 1D results, *Mon. Weather Rev.*, *132*, 864–882.
- Charlson, R. J., S. E. Schwartz, J. M. Hales, R. D. Cess, J. A. Coakley Jr., J. E. Hansen, and D. J. Hoffman (1992), Climate forcing by anthropogenic aerosols, *Science*, *255*, 423–430, doi:10.1126/science.255.5043.423.
- Chen, G., Y. Ming, N. Singer, and J. Lu (2010a), Aerosol-induced Changes in Mean and Extreme Precipitation, *Geophys. Res. Lett.*, *38*, doi:10.1029/2010GL046435.
- Chen, W.-T., A. Nees, H. Liao, P. J. Adams, J.-L. F. Li, and J. H. Seinfeld (2010b), Global climate response to anthropogenic aerosol indirect effects: Present day and year 2100, *J. Geophys. Res.*, *115*, 12,207–12,207, doi:10.1029/2008JD011619.
- Christensen, J. H., et al. (2007), Regional Climate Projections, in *Climate Change 2007: The Physical Science Basis: Contribution of Working Group I to the Fourth Assessment Report of the Intergovernmental Panel on Climate Change*, edited by S. Solomon et al., pp. 847–940, Cambridge Univ. Press, New York.
- Clarke, L., J. Edmonds, H. Jacoby, H. Pitcher, J. Reilly, and R. Richels (2007), Scenarios of Greenhouse Gas Emissions and Atmospheric Concentrations. Sub-report 2.1A of Synthesis and Assessment Product 2.1 by the U.S. Climate Change Science Program and the Subcommittee on Global Change Research. Department of Energy, Office of Biological & Environmental Research, Washington, 7 DC, USA, 154 pp.
- Costantino, L., and F.-M. Bréon (2010), Analysis of aerosol-cloud interaction from multi-sensor satellite observations, *Geophys. Res. Lett.*, *37*, L11801, doi:10.1029/2009GL041828.
- Delworth, T. L., et al. (2006), GFDL’s CM2 Global Coupled Climate Models. Part I: Formulation and Simulation Characteristics, *J. Clim.*, *9*(5), doi:10.1175/JCLI3629.1.
- Donner, L. J. (1993), A cumulus parameterization including mass fluxes, vertical momentum dynamics, and mesoscale effects, *J. Atmos. Sci.*, *50*(6), 889–906.
- Donner, L. J., et al. (2011), The dynamical core, physical parameterizations, and basic simulation characteristics of the atmospheric component AM3 of the GFDL Global Coupled Model CM3, *J. Clim.*, *24*(13), doi:10.1175/2011JCLI3955.1.
- Fang, Y., A. M. Fiore, L. W. Horowitz, A. Gnanadesikan, I. Held, G. Chen, G. Vecchi, and H. Levy (2011), The impacts of changing transport and precipitation on pollutant distributions in a future climate, *J. Geophys. Res.*, *116*, D18303, doi:10.1029/2011JD015642.
- Forster, P., et al. (2007), Changes in atmospheric constituents and radiative forcing, in *Climate Change 2007: The Physical Science Basis: Contribution of Working Group I to the Fourth Assessment Report of the Intergovernmental Panel on Climate Change*, edited by S. Solomon et al., pp. 129–234, Cambridge Univ. Press, New York.
- Griffies, S. M., et al. (2011), The GFDL CM3 Coupled Climate Model: Characteristics of the ocean and sea ice simulations, *J. Clim.*, *24*(13), doi:10.1175/2011JCLI3964.1.
- Golaz, J.-C., M. Salzmann, L. J. Donner, L. W. Horowitz, Y. Ming, and M. Zhao (2011), Sensitivity of the aerosol indirect effect to subgrid variability in the cloud parameterization of the GFDL Atmosphere General Circulation Model AM3, *J. Clim.*, *24*(13), doi:10.1175/2010JCLI3945.1.
- Guo, H., J.-C. Golaz, and L. J. Donner (2011), Aerosol effects on stratocumulus water paths in a PDF-based parameterization, *Geophys. Res. Lett.*, *38*, L17808, doi:10.1029/2011GL048611.
- Hansen, J., M. Sato, P. Kharecha, and K. von Schuckmann (2011), Earth’s energy imbalance and implications, *Atmos. Chem. Phys.*, *11*, 13421–13449, doi:10.5194/acp-11-13421-2011.
- Horowitz, L. W. (2006), Past, present, and future concentrations of tropospheric ozone and aerosols: Methodology, ozone evaluation, and sensitivity to aerosol wet removal, *J. Geophys. Res.*, *111*, D22211, doi:10.1029/2005JD006937.
- Horowitz, L. W., et al. (2003), A global simulation of tropospheric ozone and related tracers: description and evaluation of MOZART, version 2, *J. Geophys. Res.*, *108*(D24), 4784, doi:10.1029/2002JD002853.
- Keeling, C. D. (1960), The Concentration and Isotopic Abundances of Carbon Dioxide in the Atmosphere, *Tellus*, *12*, 200–203.
- Kiehl, J. T. (2007), Twentieth century climate model response and climate sensitivity, *Geophys. Res. Lett.*, *34*, L22210, doi:10.1029/2007GL031383.
- Kloster, S., F. Dentener, J. Feichter, F. Raes, U. Lohmann, E. Roeckner, and I. A. Fischer-Bruns (2010), GCM study of future climate response to aerosol pollution reductions, *Clim. Dyn.*, *34*, 1177–1194, doi:10.1007/s00382.
- Knutti, R. (2008), Why are climate models reproducing the observed global surface warming so well?, *Geophys. Res. Lett.*, *35*, L18704, doi:10.1029/2008GL034932.
- Koch, D. M., S. Menon, A. Del Genio, R. Ruedy, I. Alienov, G. A. Schmidt (2009), Distinguishing Aerosol Impacts on Climate over the Past Century, *J. Climate*, *22*, 2659–2677, doi:10.1175/2008JCLI2573.1.
- Lamarque, J.-F., et al. (2010), Historical (1850–2000) gridded anthropogenic and biomass burning emissions of reactive gases and aerosols: Methodology and application, *Atmos. Chem. Phys.*, *10*, 7017–7039, doi:10.5194/acp-10-7017-2010.
- Lamarque, J.-F., G. Kyle, M. Meinshausen, K. Riahi, S. Smith, D. Vuuren, A. Conley, F. Vitt (2011), Global and regional evolution of short-lived radiatively-active gases and aerosols in the Representative Concentration Pathways, *Clim. Chang.*, *109*(1), 191–212.
- Le Treut, H. (2012), Greenhouse Gases, Aerosols and Reducing Future Climate Uncertainties, *Surv. Geophys.*, *33*, 723–731, doi:10.1007/s10712-012-9190-2.

- Levy, H., II, M. D. Schwarzkopf, L. Horowitz, V. Ramaswamy, and K. L. Findell (2008), Strong sensitivity of late 21st Century climate to projected changes in short-lived air pollutants, *J. Geophys. Res.*, *113*, D06102, doi:10.1029/2007JD009176.
- Liao, H., Y. Zhang, W.-T. Chen, F. Raes, and J. H. Seinfeld (2009), Effect of chemistry-aerosol-climate coupling on predictions of future climate and future levels of tropospheric ozone and aerosols, *J. Geophys. Res.*, *114*, D10306, doi:10.1029/2008JD010984.
- Lohmann, L. R. U., T. Storelvmo, A. Jones, S. Menon, J. Quaas, A. Ekman, D. Koch, and R. Ruedy (2010), Total aerosol effect: radiative forcing or radiative flux perturbation?, *Atmos. Chem. Phys.*, *10*, 3235–3246.
- Meinshausen, M., et al. (2011), The RCP Greenhouse Gas Concentrations and their Extension from 1765 to 2300, *Clim. Chang.* (Special Issue), doi:10.1007/s10584-011-0156.
- Ming, Y., and V. Ramaswamy (2009), Nonlinear Climate and Hydrological Responses to Aerosol Effects, *J. Clim.*, *22*, 1329–1339, doi:10.1175/2008JCLI2362.
- Ming, Y., and V. Ramaswamy (2011), A Model Investigation of Aerosol-induced Changes in Tropical Circulation, *J. Clim.*, *24*, 5125–5133, doi:10.1175/2011JCLI4108.1.
- Ming, Y., V. Ramaswamy, and G. Chen (2011), A Model Investigation of Aerosol-induced Changes in Boreal Winter Extratropical Circulation, *J. Clim.*, doi:10.1175/2011JCLI4111.1.
- Ming, Y., V. Ramaswamy, L. J. Donner, and V. T. J. Phillips (2006), A new parameterization of cloud droplet activation applicable to general circulation models, *J. Atmos. Sci.*, *63*(4), doi:10.1175/JAS3686.1.
- Ming, Y., V. Ramaswamy, L. J. Donner, V. T. J. Phillips, S. A. Klein, P. A. Ginoux, and L. W. Horowitz (2007), Modeling the Interactions between Aerosols and Liquid Water Clouds with a Self-consistent Cloud Scheme in a General Circulation Model, *J. Atmos. Sci.*, *64*, 1189–1209.
- Ming, Y., V. Ramaswamy, P. A. Ginoux, and L. W. Horowitz (2005), Direct Radiative Forcing of Anthropogenic Organic Aerosol, *J. Geophys. Res.*, *110*, doi:10.1029/2004JD005573.
- Ming, Y., V. Ramaswamy, and G. Persad (2010), Two Opposing Effects of Absorbing Aerosols on Global-mean Precipitation, *Geophys. Res. Lett.*, *37*, doi:10.1029/2010GL042895.
- Nakicenovic, N., and R. Swart (Eds.) (2000), Special Report on Emissions Scenarios: A Special Report of Working Group III of the Intergovernmental Panel on Climate Change, 599 pp., Cambridge Univ. Press, New York.
- Neffel, A., Moor, E., Oeschger, H., and Stauffer, B. (1985), Evidence from polar ice cores for the increase in atmospheric CO<sub>2</sub> in the past two centuries, *Nature*, *315*, 45–47.
- Ocko, I. B., V. Ramaswamy, P. Ginoux, Y. Ming, and L. W. Horowitz (2012), Sensitivity of scattering and absorbing aerosol direct radiative forcing to physical climate factors, *J. Geophys. Res.*, *117*, D20203, doi:10.1029/2012JD018019.
- Penner, J. E., et al. (2001), Aerosols, their direct and indirect effects, in *Climate Change 2001: The Scientific Basis: Contribution of Working Group I to the Third Assessment Report of the Intergovernmental Panel on Climate Change*, edited by J. T. Houghton et al., pp. 289–348, Cambridge Univ. Press, Cambridge, U.K.
- Putman, W. M., and S.-J. Lin (2007), Finite-volume transport on various cubed-sphere grids, *J. Comput. Phys.*, *227*(1), 55–78.
- Quaas, J., O. Boucher, N. Bellouin, and S. Kinne (2008), Satellite-based estimate of the direct and indirect aerosol climate forcing, *J. Geophys. Res.*, *113*, D05204, doi:10.1029/2007JD008962.
- Quaas, J., et al. (2009), Aerosol indirect effects — General circulation model intercomparison and evaluation with satellite data, *Atmos. Chem. Phys.*, *9*, 8697–8717, doi:10.5194/acp-9-8697-2009.
- Ramanathan, V., P. J. Crutzen, J. T. Kiehl, and D. Rosenfeld (2001), Aerosols, climate, and the hydrological cycle, *Science*, *294*(5549), 2119–2124.
- Ramaswamy, V., et al. (2001), Radiative forcing of climate change, in *Climate Change 2001: The Scientific Basis: Contribution of Working Group I to the Third Assessment Report of the Intergovernmental Panel on Climate Change*, edited by J. T. Houghton et al., pp. 349–416, Cambridge Univ. Press, Cambridge, U.K.
- Randall, D. A., et al. (2007), Climate Models and Their Evaluation, in *Climate Change 2007: The Physical Science Basis: Contribution of Working Group I to the Fourth Assessment Report of the Intergovernmental Panel on Climate Change*, edited by S. Solomon et al., pp. 589–662, Cambridge Univ. Press, New York.
- Rayner, N. A., D. E. Parker, E. B. Horton, C. K. Folland, L. V. Alexander, D. P. Rowell, E. C. Kent, and A. Kaplan (2003), Global analyses of sea surface temperature, sea ice, and night marine air temperature since the late nineteenth century, *J. Geophys. Res.*, *108*(D14), 4407, doi:10.1029/2002JD002670.
- Schwarzkopf, M. D., and V. Ramaswamy (2008), Evolution of stratospheric temperature in the 20th Century, *Geophys. Res. Lett.*, *35*, L03705, doi:10.1029/2007GL032489.
- Shevliakova, E., et al. (2009), Carbon cycling under 300 years of land use change: Importance of the secondary vegetation sink, *Global Biogeochem. Cycles*, *23*, GB2022, doi:10.1029/2007GB003176.
- Shindell, D. T., and G. Faluvegi (2009), Climate response to regional radiative forcing during the twentieth century, *Nat. Geosci.*, *2*, 294–300, doi:10.1038/ngeo473.
- Shindell, D. T., G. Faluvegi, D. M. Koch, G. A. Schmidt, N. Unger, and S. E. Bauer (2009), Improved Attribution of Climate Forcing to Emissions, *Science*, 716–718, doi:10.1126/science.1174760.
- Shindell, D., M. Schulz, Y. Ming, T. Takemura, G. Faluvegi, and V. Ramaswamy (2010), Spatial scales of climate response to inhomogeneous radiative forcing, *J. Geophys. Res.*, *115*, D19110, doi:10.1029/2010JD014108.
- Shindell, D. T., A. Voulgarakis, G. Faluvegi, and G. Milly (2012), Precipitation response to regional radiative forcing, *Atmos. Chem. Phys.*, *12*, 6969–6982.
- Shine, K. P., et al. (1990), Radiative forcing of climate, in *Climate Change: The IPCC Scientific Assessment*, edited by J. T. Houghton, G. J. Jenkins, and J. J. Ephraums, 365 pp., Cambridge Univ. Press, New York.
- Shine, K. P., et al. (1995), Radiative forcing, in *Climate Change (1994) Radiative Forcing of Climate Change and An Evaluation of the IPCC IS92 Emission Scenarios*, edited by J. T. Houghton et al., 339 pp., Cambridge Univ. Press, New York.
- Small, J. D., P. Y. Chuang, G. Feingold, and H. Jiang (2009), Can aerosol decrease cloud lifetime?, *Geophys. Res. Lett.*, *36*, L16806, doi:10.1029/2009GL038888.
- Smith, S. J., and T. M. L. Wigley (2006), Multi-Gas Forcing Stabilization with the MiniCAM, *Energy J.* (Special Issue #3), 373–391.
- Taylor, K. E., D. Williamson, and F. Zwiers (2000), The sea surface temperature and sea-ice concentration boundary conditions for AMIP II simulations, PCMDI Report No. 60, Program for Climate Model Diagnosis and Intercomparison, Lawrence Livermore National Laboratory, Livermore, California, 25 pp.
- Thomson, A. M., et al. (2011), RCP4.5: a pathway for stabilization of radiative forcing by 2100, *Clim. Change*, *109*, 77–94, doi:10.1016/s10584-011-0151-4.
- Wang, C., D. Kim, A. M. L. Ekman, M. C. Barth, and P. J. Rasch (2009), Impact of anthropogenic aerosols on Indian summer monsoon, *Geophys. Res. Lett.*, *36*, L21704, doi:10.1029/2009GL040114.
- Winton, M., A. Adcroft, S. M. Griffies, R. W. Hallberg, L. W. Horowitz, and R. J. Stouffer (2012), Influence of ocean and atmosphere components on simulated climate sensitivities, *J. Climate*, doi:10.1175/JCLI-D-12-00121.1, in press.
- Wise, M. A., K. V. Calvin, A. M. Thomson, L. E. Clarke, B. Bond-Lamberty, R. D. Sands, S. J. Smith, A. C. Janetos, and J. A. Edmonds (2009), Implications of Limiting CO<sub>2</sub> Concentrations for Land Use and Energy, *Science*, *324*, 1183–1186.